4210 *Macromolecules* **2010**, *43*, 4210–4222
DOI: 10.1021/ma1003437

Macromolecules
ARTICLE

Inhomogeneities and Chain Dynamics in Diene Rubbers Vulcanized with Different Cure Systems†

J. L. Valentín,*,‡,§ P. Posadas,‡ A. Fernández-Torres,‡ M. A. Malmierca,‡ L. González,‡ W. Chassé,§ and K. Saalwächter*,§

‡*Institute of Polymer Science and Technology (CSIC), C/Juan de la Cierva 3, 28006 Madrid, Spain, and* §*Institut für Physik−NMR, Martin-Luther-Universität Halle-Wittenberg, Betty-Heimann-Strasse 7, D-06120 Halle, Germany*

Received February 11, 2010; Revised Manuscript Received March 29, 2010

ABSTRACT: In this study, we focus on qualitative differences in the network structure and dynamics of natural as well as poly(butadiene) rubber in dependence of the cure system (sulfur/accelerator or organic peroxide) used in the vulcanization process. The spatial homogeneity of the distribution of chemical and physical cross-links in the network is assessed via the quantitative measurement of proton−proton residual dipolar couplings as measured by static multiple-quantum (MQ) NMR spectroscopy at low field. The experiment also provides information on the apparent correlation time of fast segmental fluctuations that dominate chain relaxation processes at lower temperature, for which we also find characteristic differences. Vulcanization via a radical mechanism (using organic peroxides) leads to networks with a high content of nonelastic defects (loops or dangling chains), a rather inhomogeneous distribution of cross-links, and modified (slower) local dynamics, as compared to networks obtained by sulfur vulcanization. These microstructural factors can be related with the well-known differences in the macroscopic properties of diene rubbers vulcanized with different cure systems.

Introduction

Vulcanization is one of the main topics in rubber science and technology.[1−3] Historically, the term vulcanization referred to the process of heating rubber, sulfur, and white lead. By terminology, the cross-linking process of rubber is often called vulcanization when it involves the use of sulfur or sulfur compounds. Nevertheless, vulcanization is nowadays generally understood as the process of forming three-dimensional networks by random linking of linear elastomers by chemical or physical methods.[4,5]

Even more than 150 years after the discovery of the vulcanization by Thomas Hancock and Charles Goodyear, who found that a plastic rubber polymer could be transformed into an elastic material by the addition of sulfur and heat, the reaction mechanisms are not completely understood. Sulfur vulcanization is still the most-used curing system in rubber industry,[6−9] nevertheless, discussions concerning the nature of the reaction (ionic or free radical) that govern the process are still ongoing.[7,9−11] Several works concluded that both mechanisms are operative and that their relative importance depends on the formulation, type of rubber or vulcanization conditions.[7,9−11]

The simplest formulation, i.e., the mere addition of sulfur, produces the most complex network. Sulfur reacts with rubber chains creating sulfur cross-links of different lengths (mainly polysulfidic bonds), pendant side groups, cyclic sulfides, and changing the polymer backbone structure, e.g., cis/trans isomerizations of the double bonds and/or conjugated sequences.[3] The low reaction efficiency, in addition to the long time required to complete the vulcanization process, are the reasons that just sulfur without accelerator is not in use for commercial purposes (excluding maybe ebonite).

A substantial development in the rubber industry emerged with the use of accelerators (generally organic molecules).[12] Accelerated sulfur vulcanizations are classified as conventional (CV), semiefficient (semi-EV) and efficient (EV) vulcanization, depending on the accelerator/sulfur ratio (denoted A/S in the following) usually ranging between 0.2 and 12. The mechanism remains undisclosed and even essential aspects are unknown. In practice, the process of vulcanization is subdivided into three stages.[9,10] The first one involves the "accelerator chemistry" where the reactions lead to the formation of an active sulfuration agent. A second stage comprises the "chemistry of cross-linking", which includes reactions leading to the formation of cross-links, and finally the "post-cross-linking chemistry", involving reactions leading to shortening and degradation of chains and cross-links.[13,14] Although the chemistry of the process is not well understood, the consequences for the network structure are well described, e.g., an increase of the accelerator/sulfur ratio reduces the length of the sulfur bridges and increases the number of cross-links; hence the elastic properties of the compounds are modified.

An alternative to sulfur cure systems in rubber industry is the vulcanization with organic peroxides.[13] In this case, the reaction pathway is clearly radical. Peroxide vulcanization is initiated by the thermal homolytic scission of the peroxide molecule, forming two radicals. These radicals can remove more labile allylic hydrogen atoms from the polymer or can be added to double bonds (in the case of unsaturated elastomers), forming randomly polymeric macro-radicals. Finally, two competing termination reactions may take place:[15−18] (i) recombination of two macro-radicals into one tetra-functional carbon−carbon cross-link per peroxide molecule or (ii) addition of one macro-radical to a double bond giving rise to a cross-link and a new active macro-radical, which can react again with another neighboring chain.

† This paper is dedicated to Prof. Luis González, inspiration for this work, on the occasion of his retirement

*Corresponding authors. E-mail: (J.L.V.) jlvalentin@ictp.csic.es; (K.S.) kay.saalwaechter@physik.uni-halle.de.

 Published on Web 04/15/2010

Although much empirical information related to the determination of vulcanization mechanisms, activation energies, and kinetic constants of the involved reactions have been reported[10] based on chemical analysis, high-resolution solid-state NMR, mass spectrometry, ESR, DSC, and gas chromatography, the issue must still be considered unresolved. Obviously, chemical reactions involved in vulcanization processes determine the elastomer network structure and therefore their elastic properties. As long as the detailed reaction pathways of the most-used processes in rubber technology are unclear and remain too complex to be unveiled, the most useful approach to control and to be able to obtain tailor-made properties of elastomeric materials is clearly the direct study of the mesoscale network structure formed during the vulcanization reactions.

The long-range elasticity is the main characteristic of elastomers.[19−21] Numerous molecular attempts have been made to describe the thermodynamics of the stress−strain relationship exhibited by elastomeric materials. Early molecular models, i.e. affine[22] and phantom network models,[23,24] are based on (i) an entropic origin of the elastic restoring force exhibited by a deformed network and (ii) a Gaussian distribution function for the end-to-end distances of the network chains. According to these statements, the total stress at a given deformation should only depend on the number of cross-links and their functionality.[25]

Although both models give a good qualitative picture of rubber elasticity, a more quantitative treatment was only possible with topological interactions between network chains taken into account, demonstrating the important contribution of entanglements to rubber elasticity. Initially, in the constrained-junction model[26,27] the confining potential produced by neighboring chains acts only through junction points. Later models, e.g., Edwards tube model,[28] nonaffine tube model,[29] or the slip-tube model,[30,31] extend the topological constrains to the whole contour of the network strand, confining the segmental polymer chain fluctuations into a confining tube.

In conclusion, following any of the molecular approaches,[32] it is possible to qualitatively describe the rubber properties by studying the number of elastically active cross-links, their functionality and entanglements. Nevertheless, elastomer networks are not ideal at all; hence it is important to take also into consideration two more network parameters: (i) the number of defects,[31] i.e., chain segments that are elastically nonactive such as free chain ends, dangling chains or loops, and (ii) the spatial cross-link distribution,[33,34] since the formation of cross-links during the vulcanization process could be not completely random and therefore inhomogeneities in rubber networks may be relevant.

Information on the rubber network structure can be obtained by different experimental approaches, such as inverse gas chromatography,[35] osmometry,[36] mechanical analysis,[37] equilibrium swelling experiments,[38] dielectric measurements,[39] high-resolution solid-state NMR,[40,41] or scattering techniques.[42,43] Often, however, such approaches are indirect. For instance, in recent work,[44] two different phase components with different cross-link density in sulfur cross-linked natural rubber (NR) samples were deduced from strain-induced crystallization studies. For length scales of a few nm or larger, this statement will be proven wrong in this manuscript, demonstrating the value of direct methods such as the one used herein, namely time-domain proton solid-state NMR spectroscopy.

Time-domain solid-state NMR spectroscopy has demonstrated to be one of the most powerful and versatile tools to investigate polymer networks.[45−49] In fact, it is able to provide a fascinating wealth of information on structure and dynamics in elastomers. Cross-links and other topological constrains restrict the number of accessible chain conformations, which leads local chain ordering caused by the nonisotropic chain motions. In consequence, residual dipolar couplings, which are the NMR observable, persist. Different experimental NMR approaches, e.g., ^{1}H transverse relaxation experiments,[50] combinations of Hahn and solid echoes,[51] or two-dimensional (2D) magnetization exchange spectroscopy,[52] were used to evaluate various parameters governed by the residual dipolar coupling interactions. It has been demonstrated that proton double-quantum (DQ) (or more generally multiple-quantum, MQ) NMR, that makes a more direct use of the dipolar couplings, can be considered as the most quantitative and reliable method for the measurement of residual dipolar couplings.[49] As opposed to the recently criticized measurements of transverse relaxation times,[50,53] MQ NMR experiments provide two sets of data which can be used to independently analyze the coherent dipolar effect independent of any assumptions on the spin−spin relaxation phenomena induced by random thermal motions. Inhomogeneity of networks is assessed via analyzing the data in terms of distributions of residual couplings. Our earlier work has shown that trivially expected distributions in chain length and end-to-end distance are not detectable in terms of residual coupling distributions,[54] while actual spatial inhomogeneities arising from changes in the average density of cross-links on the scale of a few nm and above are faithfully detected.[54,55]

The objective of the present work is to study the differences in the network structure and dynamics of natural as well as poly(butadiene) rubber as a function of the vulcanization system (sulfur/accelerator or organic peroxide) by using ^{1}H DQ NMR experiments performed at low field. We demonstrate that the rubber matrix of sulfur vulcanizates is in fact spatially very homogeneous, while peroxide-based cross-linking leads to large spatial variations in the cross-link distribution as well as higher fractions of elastically inactive defects.

Experimental Section

Materials and Preparation of Samples. The studied compounds were based on standardized poly(*cis*-1,4-isoprene) natural rubber (NR), kindly supplied by Malaysian Rubber (SMR-CV60), and poly(*cis*-1,4-butadiene) rubber (BR) with 98% *cis*-1,4 structures, obtained from Polimeri Europa.

Three different cure systems were used in both NR and BR: conventional (C), efficient (E) and peroxide-based (P). The first two are based on sulfur-accelerator recipes and they contain zinc oxide (5 parts per hundred of rubber, phr) and stearic acid (2 phr) as activators, and different amounts of the accelerator *N*-cyclohexyl-2-benzothiazolesulphenamide (CBS) and sulfur. The differences between both systems are just the A/S and the sulfur content. In the conventional cure system the A/S was always 0.2 with increasing sulfur content: 0.7; 1.3; 1.9; 2.5; 3.1; 3.7; 7.4, and 11.1 phr. The efficient cure system has a lower amount of sulfur, e.g., 0.1; 0.24; 0.4; 0.56; 0.7, and 0.84 phr, but a higher A/S of 12. Finally, peroxide based recipes only contain rubber and an increasing amount of dicumyl peroxide (DCP), e.g., 0.5, 1, 2, 3, 4, 6, 8, 10, and 12 phr. Note that in peroxide vulcanization, BR samples only contain 0.5, 1, 2, and 3 phr of DCP because higher peroxide contents leads to networks with excessively high cross-link densities that are beyond our experimental range (and beyond practical use).

The sample names, e.g., NR-C(1.3) encode the type of rubber (NR), the vulcanization system (C = conventional) and the amount of sulfur or peroxide in phr (1.3 in this case). The samples were prepared in an open two-roll mill using standard mixing procedures and vulcanized in a laboratory press at 150 °C at their respective optimum times (t_{97}), deduced from the rheometer curve (Monsanto moving die rheometer, model MDR 2000E).

^{1}H Double Quantum (DQ) Solid-State NMR Experiments. DQ (or more generally MQ) spectroscopy is one of the most versatile and robust quantitative techniques to investigate not only the structure but also the dynamics of polymer networks.[49] In this work, experiments were carried out on a Bruker minispec mq20 spectrometer operating at 0.5 T with 90° pulses of 1.7 μs

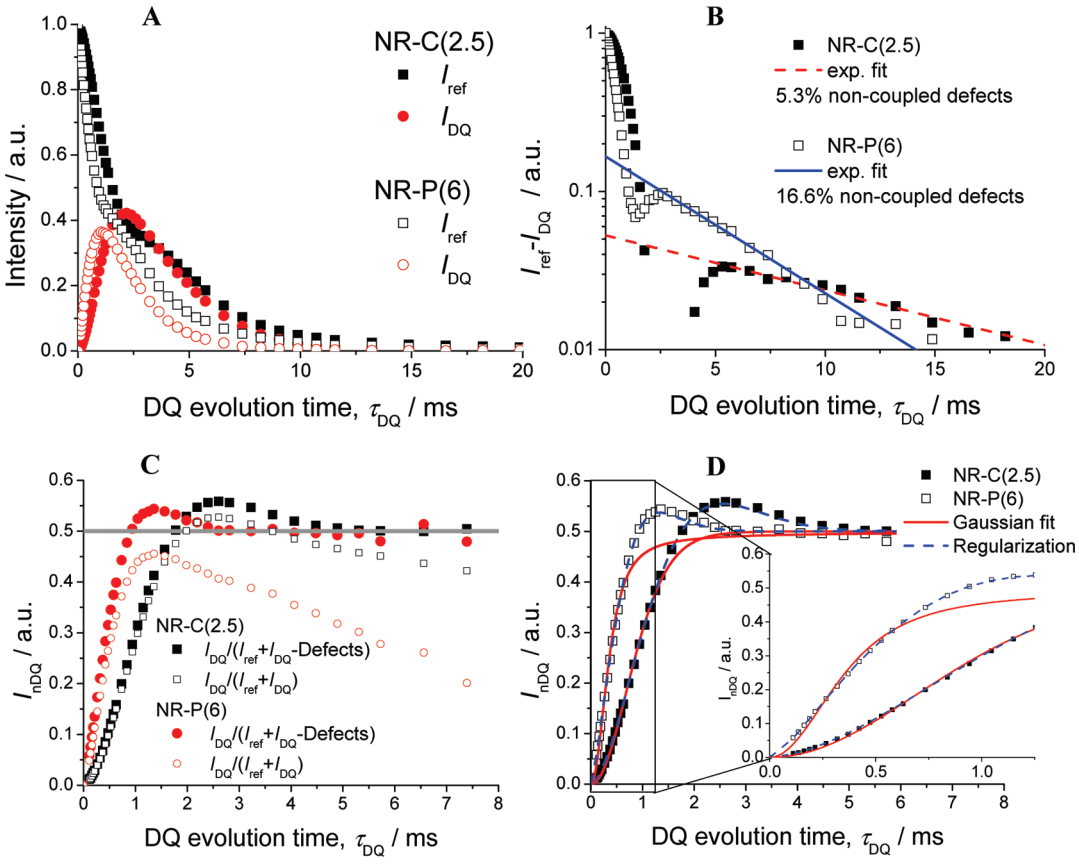

Figure 1. Regularization procedure and data analysis of two studied samples. In part A, the raw DQ build-up (I_{DQ}) and reference decay (I_{ref}) data are represented as a function of the double-quantum evolution time τ_{DQ}. I_{ref}, or better the difference $I_{ref} - I_{DQ}$, can be used to identify the more slowly relaxing nonelastic (isotropically mobile) defect fraction (B). The fraction of nonelastic network defects has to be subtracted to obtain a proper point-by-point normalization of the DQ intensity (C). I_{nDQ} is now independent of temperature-dependent true relaxation (decay) effects and it reaches the expected plateau value of 0.5 (reflecting the equal partitioning among higher quantum orders between I_{DQ} and I_{ref}). Finally I_{nDQ} is used to analyze the residual dipolar coupling and its distribution (D). I_{nDQ} can be fitted under the assumption of a Gaussian distribution of dipolar couplings. Nevertheless in some cases (e.g., NR−P(6)) the fit cannot reproduce the initial rise well, indicating wider or multimodal coupling distributions. In these cases, a numerical inversion procedure is resorted to.

length and a dead time of 12 μs. The experiments and the data analysis were performed following the previously published procedures.[49]

For a cursory explanation of the principles, it is important to consider the time-dependent orientation autocorrelation function expected for segments in a polymer network. Initially, segments lose their orientational memory via fast local fluctuations (higher Rouse modes). Eventually, topological restrictions (entanglements) and the permanent cross-links constrain the lower and longer-ranged modes, leading to a long-time plateau in the orientation autocorrelation function. This is to say that the restrictions give rise to segmental fluctuations that are nonisotropic at long times, and, in consequence, a residual local order persists. Further loss of correlation as a result of slow cooperative dynamics, as for instance expected from reptation processes in long-chain melts, have been repeatedly invoked, but have unambiguously been demonstrated to be not relevant in rubber networks.[56] Therefore, two main parameters are relevant: (i) the plateau value of the orientation autocorrelation function, which is given by the square of the dynamic residual order parameter of the polymer backbone, S_b, and (ii) a correlation time τ_f that characterizes the time scale of the initial decay of orientation correlations, caused by the fast local modes. S_b is directly related to the network structure, as it is directly proportional to the cross-link density. It is obtained directly from the measurement, because the experimental residual dipolar coupling is also directly proportional to S_b.

In the high temperature regime, the data from MQ experiments can be processed in such a way that the temperature-independent network structure effect (S_b) can be separated from the temperature-dependent segmental dynamics without invoking any specific model. This involves a normalization procedure using the two sets of experimental data, the DQ build-up (I_{DQ}) and reference decay (I_{ref}) curves, that are both measured as a function of the double-quantum evolution time τ_{DQ}, which represents the variable duration of the pulse sequence (Figure 1A). The sum of both components ($I_{DQ} + I_{ref}$) comprises the full magnetization of the sample, i.e., signal from dipolar coupled network segments (including DQ and higher-order coherences as well as dipolar-encoded longitudinal magnetization), and signal from uncoupled, i.e., isotropically mobile network defects, e.g., dangling chains and loops (note that protons in solid-like environments such as proteins or lipid clusters in NR, crystallized stearic acid chains, etc., are not detected in this experiment; their relative contribution to the overall signal is low in any way). The individual fractions are characterized by rather different relaxation behavior, which can even be even amplified by plotting $I_{ref} - I_{DQ}$ (Figure 1B). Coupled (network) segments relax faster and typically in a nonexponential fashion, while the signal of noncoupled, elastically nonactive defects show a slower exponential decay (T_2^* in eq 1 below). Therefore, it is necessary to identify and subtract the exponential long-time contribution (i.e., the noncoupled fraction of polymer chains termed B in eq 1) to the total MQ magnetization, $I_{\Sigma MQ}$:

$$I_{\Sigma MQ} = I_{DQ} + I_{ref} - B\mathrm{e}^{-2\tau_{DQ}/T_2^*} \quad (1)$$

After the identification and subtraction of the nonelastic network defects (Figure 1B), the total MQ magnetization, $I_{\Sigma MQ}$, is used to normalize the DQ intensity point-by point ($I_{nDQ} = I_{DQ}/I_{\Sigma MQ}$). I_{nDQ} is now independent of any temperature-dependent

true relaxation (decay) effect and it has to reach a plateau value at 0.5, because I_{DQ} only contains half of the excited quantum orders (Figure 1C). This behavior is only observed after proper identification and subtraction of nonelastic network defects (see Figure 1C), hence the observation of the plateau behavior proves the internal consistency of the analysis. Therefore, I_{nDQ} is dominated by the dipolar interactions that are only related with the network structure (i.e., proportional to S_b). To evaluate not only the dipolar interactions, but also possible distribution effects, I_{nDQ} can be fitted under the assumption of a Gaussian distribution of dipolar couplings,[49]

$$I_{nDQ}(D_{res},\sigma) = \frac{1}{2}\left(1 - \frac{\exp\left\{-\frac{\frac{2}{5}{D_{res}}^2{\tau_{DQ}}^2}{1+\frac{4}{5}\sigma^2{\tau_{DQ}}^2}\right\}}{\sqrt{1+\frac{4}{5}\sigma^2{\tau_{DQ}}^2}}\right) \quad (2)$$

which yields both an *average* apparent coupling constant (D_{res}) and its standard deviation (σ) characterizing the distribution width, both in units of rad/s. A numerical inversion procedure based on eq 2 with $\sigma \rightarrow 0$ as Kernel function and fast Tikhonov regularization,[57,58] was previously used to obtain a quantitative picture of the actual distribution function of residual couplings.[55] When samples show narrow distributions of dipolar couplings both fitting procedures give the same result and perfectly define the initial rise of I_{nDQ}, as seen for sample NR-C(2.5) in Figure 1D. However, in samples where the distribution effects are more significant (e.g., broader distribution or inhomogeneities in the spatial distribution), the initial rise of the experimental build-up cannot be described by the Gaussian fit (eq 2), as is particularly apparent for the NR-P(6) sample in Figure 1D. In such cases, the regularization procedure is the preferred approach.

In this manuscript, a modified version of the numerical fit was used, which is based on an improved Kernel function that describes the local maximum in data of homogeneous networks, enabling a fit of the full build-up curve and not just the initial rise, thus providing reliable and precise results. Details are deferred to the Appendix and will also be addressed in an upcoming publication.

Note that the experiment is performed without chemical resolution, which means that all proton types are detected simultaneously and the resulting D_{res} represents an average over different internuclear, intramonomer pair couplings (it is a second-moment-type quantity). It is related to S_b via the following expression[49]

$$S_b = k\frac{D_{res}}{D_{stat}} = \frac{3}{5}\frac{r^2}{N} \quad (3)$$

where k represents the local coupling topology and intrasegmental motions that should be used to rescale the static coupling constant, D_{stat}, (determined by the fixed proton−proton distances) in order to account for averaging effects that occur on the level below the segmental (Kuhn) length. From previous spin dynamics simulations, and assuming a reasonable model for the intrasegmental motions, apparent reference couplings for natural rubber and cis-polybutadiene were obtained:[59] $D_{stat}^{(NR)}/k = 2\pi \times 6300$ Hz and $D_{stat}^{(cis-BR)}/k = 2\pi \times 8100$ Hz, respectively.

Equation 3 relates S_b and the NMR observable, D_{res}, with the ratio of the end-to-end vector to its average unperturbed melt state ($r^2 = \boldsymbol{r}^2/\langle \boldsymbol{r}^2\rangle_0$), and with N, which represents the number of statistical (Kuhn) segments between constrains. Therefore, by using the definitions of Flory's characteristic ratio and the Kuhn segment length (and assuming an extended chain conformation within the Kuhn segment), it is possible to obtain the relationship between experimental D_{res} and the molecular weight between constrains, M_c, in both NR and cis-BR samples:

$$M_c^{(NR)} = \frac{617\ \text{Hz}}{D_{res}/2\pi}\,\text{kg/mol}$$

and

$$M_c^{(cis-BR)} = \frac{656\ \text{Hz}}{D_{res}/2\pi}\,\text{kg/mol}$$

respectively. This magnitude is related to the cross-link density (assuming tetra-functional cross-links) by the expression

$$\nu_{NMR} = \frac{1}{2M_c}$$

The approximate validity of our (model-dependent) reference values has recently been confirmed by comparison with results from equilibrium swelling experiments.[38]

While I_{nDQ} depends only on structural factors and does not show any temperature dependence (at least when no significant fraction of entangled high molar mass defects is present), the directly obtained build-up (I_{DQ}) and decay functions ($I_{\Sigma MQ}$) of the MQ experiments always exhibit a marked temperature dependence. They thus reflect the dynamic processes represented by the fast segmental modes. Assuming a homogeneous network structure ($\sigma = 0$ in eq 2), and using the Andersen−Weiss (AW) approximation in combination with a rather simplistic model of an exponential loss of correlation described by $C(t) = {S_b}^2 + (1 - S_b)^2\exp\{-t/\tau_f\}$, it is possible to obtain simple analytical results for the signal functions,[49,56]

$$I_{DQ} = \exp\left\{-\frac{8}{9}(1-{S_b}^2)M_{2eff}{\tau_f}^2\left(e^{\tau_{DQ}/\tau_f} + \frac{\tau_{DQ}}{\tau_f} - 1\right) - \frac{4}{9}{S_b}^2M_{2eff}{\tau_{DQ}}^2\right\}\sinh\left\{\frac{4}{9}(1-{S_b}^2)M_{2eff}{\tau_f}^2(e^{-2\tau_{DQ}/\tau_f} - 2e^{-\tau_{DQ}/\tau_f} + 1) + \frac{4}{9}{S_b}^2M_{2eff}{\tau_{DQ}}^2\right\} \quad (4)$$

$$I_{\Sigma MQ} = \exp\left\{-\frac{4}{9}(1-{S_b}^2)M_{2eff}{\tau_f}^2\left(4e^{-\tau_{DQ}/\tau_f} - e^{-2\tau_{DQ}/\tau_f} + \frac{2\tau_{DQ}}{\tau_f} - 3\right)\right\} \quad (5)$$

where the residual dipolar second moment is given by

$$M_{2eff} = \frac{9}{20}{D_{res}}^2$$

Note that the quotient of these expressions, $I_{nDQ} = I_{DQ}/I_{\Sigma MQ}$, matches eq 2 with $\sigma = 0$ rather precisely over the full fast-motion range where $\tau_f \ll 1/D_{res}$.

Using these expressions, it is possible to obtain an estimate of the fast correlation time τ_f by simultaneous fitting of I_{DQ} and $I_{\Sigma MQ}$ with shared parameters. It is important to note that all fitting procedures except the improved regularization approach described in the Appendix are only valid in a time region below $\tau_{DQ}^{max} = 2.4/D_{res}$, as a consequence of the second-moment approximation used. It is also important to remark that approximating the true correlation loss (which is most likely a power law, resulting from a sum over many modes) by a single exponential is a very crude approximation, thus τ_f is merely an indicator of the average time scale of correlation loss. Our previous work has shown that the temperature dependence of τ_f nicely follows the expected WLF-type law,[56] which is expected

since the fastest segmental mode (the α relaxation time) controls the whole chain dynamics. In this way, τ_f can be used to qualitatively compare the segmental relaxation behavior of different samples.

Differential Scanning Calorimetry (DSC) Analysis. The glass transition temperature (T_g) of the NR samples was measured by using a DSC 7 instrument from Perkin−Elmer. Nitrogen gas with a flow rate of about 20 mL/min was purged through the cell. Experiments started with an isothermal step (5 min) at 25 °C, and then samples were cooled down from +25 to −120 °C at a rate of −10 °C/min. After 10 min of equilibration at that temperature, far enough below T_g, a heating rate of 10 °C/min was applied up to 25 °C, and T_g was taken from this heating run. In some rubber samples these experiments were repeated twice (with different pieces of rubber), confirming a maximum uncertainty of 0.5 °C on the measured T_g.

Results and Discussion

The main goal of this manuscript is to assess the differences in the network structure and the segmental dynamics of two types of dienic rubbers, i.e., natural rubber and *cis*-poly(butadiene), in dependence of the vulcanization system. The local structural information on the complex rubber matrix is obtained by ^{1}H solid-state MQ NMR experiments performed on low-field spectrometers. Starting with the rubber network structure, we first evaluate the influence of the different vulcanization systems and polymer type on the amount of nonelastic network defects, i.e., dangling chains and loops. Then, we discuss the efficiency of the vulcanization reaction and the effect on the spatial cross-link distribution, i.e., homogeneity or inhomogeneity of the rubber network. Finally, structural differences caused by the reactions that take place during the vulcanization process are correlated with the detected variations in the segmental dynamics, which is of course closely connected to the T_g values obtained by DSC.

1. Rubber Network Structure. Rubber is characterized by long-range elasticity. This property strongly depends on the rubber network structure obtained during the vulcanization process. According to the statements described in the Introduction, a complete description of the network structure should contain information about nonelastic network defects, number of cross-links (or the equivalent chain molecular weight between cross-links, M_c), their chemical nature and functionality, the spatial distribution of cross-links, and information about entanglements. MQ NMR experiments allow us to extract quantitative information on most of these parameters, as will be shown in this section.

1.1. Nonelastic Network Defects. Usually, rubber networks obtained by random cross-linking reactions are considered as perfect networks, in a sense that their properties can be compared to theories. Nevertheless, the importance of nonelastic network defects, mainly dangling chains and loops, is well established as to their effect on stress relaxation.[60−63] Elastomers exhibit long-term relaxation processes caused by the relaxation of pendant chains in the presence of entanglements. Pendant chains are fixed to the network structure, and therefore cannot be relaxed by reptation along the confining tube like linear entangled chains.[64] The main relaxation pathway is thus characterized by slower arm retraction processes.[65] This means that the relaxation time of pendant chains should depend on the number of topological restrictions in which they are involved. In randomly cross-linked elastomers, the relaxation behavior is strongly dependent on temperature and cross-link density, as demonstrated by stress relaxation experiments.[66,67] By using model end-linked poly(dimethylsiloxane) elastomers with controlled defect structures, the influence of concentration, molecular weight, and distribution of pendant chains on the arm retraction mechanism has been demonstrated,[68,69] providing a rationale for the mechanical relaxation processes.[62,63]

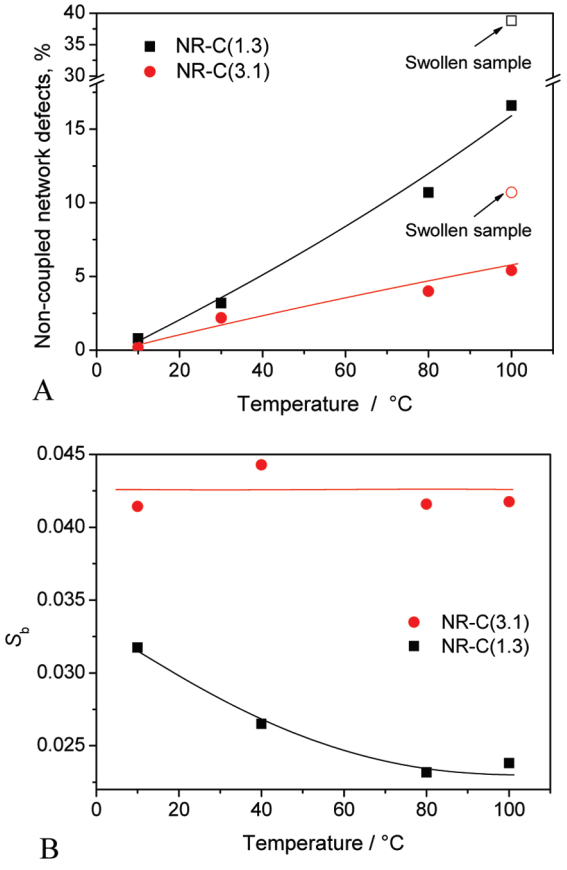

Figure 2. Evolution of the noncoupled defect fraction A and the order parameter S_b B of two studied samples (NR-C(1.3) and NR-C(3.1)) as a function of temperature. Noncoupled network defects of swollen samples were measured at 30 °C and represented as empty symbols.

With MQ NMR experiments it is possible to differentiate and quantify the fraction of noncoupled defects, i.e., chain segments with isotropic motions that ultimately average out the dipolar couplings and show slower relaxations, from the *real* polymer network, i.e., segments that are dipolar coupled because of the presence of permanent constraints (independently of the nature) that lead to permanently nonisotropic segmental motions.[49] As shown in Figure 2A, the fraction of noncoupled network defects obtained by MQ−NMR experiments shows a significant dependence on cross-link density and temperature, similar to stress relaxation experiments. At low temperature, network defects are observed as coupled segments because the entanglements restrict their motions on the experimental time scale (tens of ms). In this case, pendant chains behave as elastic network segments and NMR cannot differentiate them from the permanent network. At higher temperature, the arm retraction process (or reptation in case of linear sol) renders the motion of larger portions of the defect fraction isotropic, in consequence the apparent fraction of detected noncoupled defects increases. This is also the reason why I_{nDQ} curves (thus the average D_{res} or S_b) can become temperature-dependent in systems with high content of long defect chains, see Figure 2B.

The above interpretation is confirmed when toluene-swollen samples are analyzed. Rubber samples were swollen during 24 h in sealed dark vials, in order to protect them from light and prevent sample degradation.[38] Under these conditions, the solvent acts as plasticizer, accelerating chain

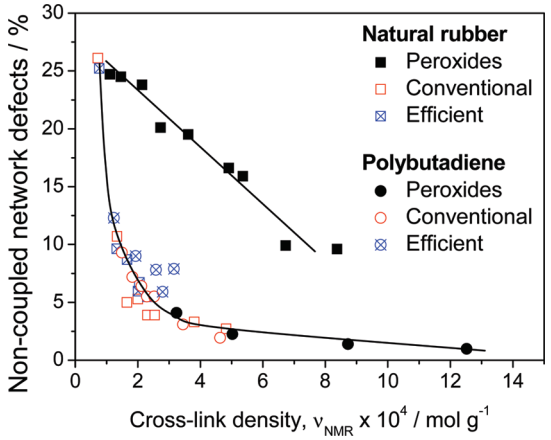

Figure 3. Evolution of the noncoupled defect fraction as a function of cross-link density for different types of rubber and vulcanization systems. Results are obtained from measurements at 80 °C. Lines are only guides to the eye.

dynamics (by shifting T_g) and thus releasing most topological constrains on the NMR time scale. This leads to a considerable increase in the detectable fraction of noncoupled (and in consequence elastically nonactive) network defects. In the two cases shown in Figure 2, the defect fraction increases by about a factor of 2 on swelling, providing an estimate of its upper limit.

In randomly cross-linked networks, the fraction of network defects also depends on the cross-link density, as shown in Figure 2A. Increasing the number of junctions (e.g., by increasing the proportion of curatives) leads to a decrease of the molecular weight of end chains, and in consequence to a decrease in the fraction of noncoupled defects (see also Figure 3). Shorter pendant chains (independently of their structure and potential molecular weight distribution, the study of which is out of the scope of this manuscript) have less topological constraints confining them; hence the dependence of detectable network defects on temperature is expected to be weaker.

NMR is not only sensitive to the cross-links but also to topological constrains, i.e. entanglements, which are equally important restrictions to the segmental motions. We can thus expect variations in the average order parameter with temperature because of the release of the entanglement constraints of the elastically active inner part of the pendant chains, which is detected along with the true network. However, we observe no significant temperature dependence of S_b for highly cross-linked samples (e.g., NR-C(3.1)), which demonstrates that these inner parts of the defect fraction exhibit a similar anisotropy of their motions as the network chains themselves, into which they are intimately embedded. The strong temperature dependence observed for the less cross-linked sample in Figure 2.B is thus partially due to the fact that the chain dynamics is not fast enough to reach the plateau value of S_b in the lower temperature range, as already shown in previous work.[49]

The (Rouse) relaxation time of the longest chain between topological restrictions (which roughly corresponds to the entanglement length at low cross-link density) is tied to the segmental relaxation time, which in turn is related to T_g. Therefore, to complete segmental averaging over all possible chain conformations on the time scale of the NMR experiment, dynamics must be fast enough; hence measurement temperatures have to be far above T_g. It is a central point to obtain the proper order parameter (hence the proper cross-link density) from the plateau range. Thus, NMR measurements were carried out at 80 °C ($T > T_g + 150$ °C).

Although at this temperature the fraction of noncoupled network defects is underestimated, it is possible to extract quantitative information from a series of samples with different cross-link density and vulcanized with different cure systems. Figure 3 shows a clear decreasing tendency of noncoupled network defects with the cross-link density because of the shortening of the molecular weight of the end chains. For this reason, most of the samples, independently of the rubber structure (NR or BR) or the vulcanization system exhibit a similar behavior, reaching values around 5% of network defects in the region of cross-link density that is useful for technical applications. From the comparison of swollen vs dry samples in Figure 2, we take that this fraction is underestimated by a factor of 2 at most.

On the other hand, NR samples vulcanized by peroxide (DCP) show a completely different behavior, with significantly larger fractions of noncoupled network defects. In the range of cross-link densities with technical applications, 15−25% of the polymer vulcanized with DCP is elastically inactive (at least at this temperature on the time scale of ms). The main reason for the high content of network defects should be ascribed to chain scissions that could take place during the vulcanization process.[70]

In this case, cross-linking and scission are sequential and competing reactions, made possible by the radical mechanism pathway characteristic of peroxide cure systems. During scission, the rearrangement of unpaired electrons in the macro-radicals causes a breakdown of the polymer backbone, leaving a double bond and a radical.[15] Nevertheless, macro-radicals are also present in BR samples vulcanized with DCP, but in this case scission seems to be much less relevant than cross-linking. In consequence, the main factor that determines the importance of chain scission over cross-linking during rubber vulcanization with peroxides seems to be the polymer backbone structure. It is actually well-known that primary or secondary radicals more readily undergo coupling reactions than tertiary ones, which undergo scission reactions instead (polyethylene and polypropylene or ethylene propylene rubber are good examples for this behavior[71,72]). In consequence, the tertiary carbons present in the NR structure are the main reason for its poor peroxide cross-linking performance.

1.2. Cross-Link Density. Although network defects are the responsible for long-term stress relaxation processes, the main property of the materials, i.e., the elasticity, is determined by the cross-links created during vulcanization. Figure 4 shows the dependence of cross-link density on the concentration of vulcanizing agent. In most of the cases, they show a linear relationship, at least in the studied range of concentrations. The only exceptions are the samples vulcanized with a conventional cure system. In this particular case, the efficiency of the vulcanization reaction seems to decrease with the amount of sulfur, leading to a nonlinear relationship. Different vulcanization systems show different reaction efficiency, as is clearly apparent from the slopes in Figure 4. Note that the *y*-intercept quantifies the contribution of (elastically active) in the total NMR-detected cross-link density. This constitutes an important advantage over other useful experimental techniques, e.g., equilibrium swelling experiments. Whereas NMR results represent the *real* number of constraints in the network, the entanglement effect on swelling experiments is complex, reducing them to the fraction that is topologically "trapped".[38] According to *y*-intercept values in Figure 4, it is possible to estimate the molecular weight between entanglements (M_e) of both NR ($M_e^{NR} \sim 6000$ g/mol) and BR ($M_e^{BR} \sim 3500$ g/mol), that are

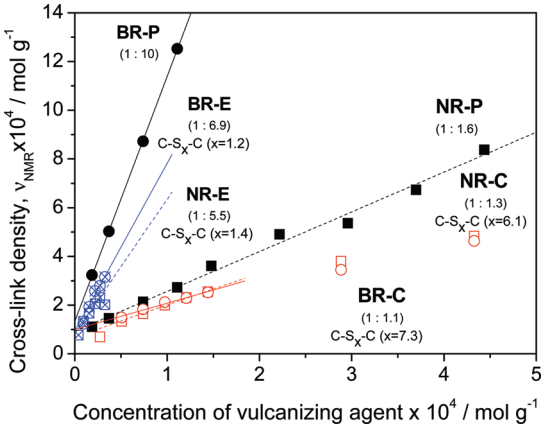

Figure 4. Efficiency of different vulcanization reactions in NR and BR samples measured as the relationship of cross-link density obtained at the optimum cure time (measured by NMR) and the concentration of vulcanizing agent. Numbers in brackets represent the slope of the linear fit. According to the slope (efficiency), it is possible to obtain crude estimates of the lengths of the sulfidic cross-links. Linear fits of samples vulcanized by the conventional system were performed in the represented range of concentration because of the loss of efficiency at higher sulfur concentrations. The *y* intercept is the (trapped) entanglement contribution to the cross-link density.

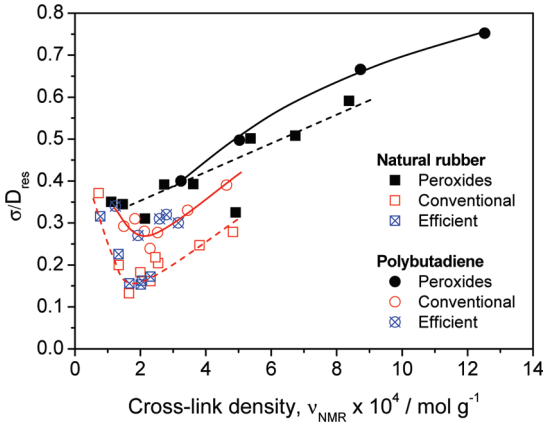

Figure 5. Variation of the relative width of the distribution of cross-link density as a function of cross-link density for the different samples and cure systems. A Gaussian distribution of cross-link density was assumed, where σ represents the standard deviation and D_{res} the average value of the distribution according to eq 2. Lines are only guides to the eye.

in reasonable agreement with other published values, $M_e^{NR} \sim 6200$ g/mol and $M_e^{BR} \sim 2300$ g/mol, respectively.[73−75]

In the sulfur-based systems, an increase in accelerator content improves the efficiency of the sulfur reaction, creating higher numbers of sulfidic cross-links with shorter lengths. According to Figure 4, networks obtained by using the efficient cure system must be formed mainly via mono- and bisulfidic cross-links, whereas the conventional vulcanization system favors larger poly sulfidic bridges. These are just crude estimations, since we assume that the vulcanizing agent is the entire sulfur molecule (i.e., eight sulfur atoms), and we consider complete conversion of sulfur (meaning that 1 mol of S_8 = 1 mol of vulcanizing agent = 1 mol of cross-links). The last statement is proven wrong, at least in the case of the conventional system, because of efficiencies below unity at higher concentration of vulcanizing agent (these samples where not taken into consideration in the linear fit represented in Figure 4). Therefore, we know that the lengths of the polysulfidic cross-links could be overestimated. Nevertheless the NMR estimation is in good agreement with the values obtained by chemical determination.[76]

It is important to note that both sulfur-based systems show similar efficiency in NR and BR, while a very different behavior is observed when peroxides are used as curing agent. In peroxide vulcanization, the amount of effective cross-links, i.e., those which create a dipolar coupled elastically active chain segment, produced per mol of peroxide molecules increases significantly in BR as compared to NR. Although in both cases the peroxide efficiency is higher that the unity, in BR samples each mol of peroxide is able to create 10 mols of effective cross-links. These results can be rationalized on the basis of the radical vulcanization mechanism of peroxides and the polymer backbone structure that contains double bonds.

Taking aside several possible side-reactions not considered here,[15] one may roughly divide the peroxide cross-linking reaction into two steps: formation of polymeric radicals, and reaction of macro-radicals creating cross-links. Two polymeric radicals can recombine in a termination reaction that creates one effective cross-link, but then, the efficiency of the reaction should be limited to the unity. However, in dienic elastomers, polymeric radicals can react also via addition to a double bond creating cross-links and new reactive radicals that can react again increasing the efficiency of the peroxide reaction. It is thus important to note the capacity of a radical to start addition chain reactions, i.e., a "polymerization" process, which greatly increases the efficiency of the vulcanization reaction.[16,18]

In consequence, the higher peroxide efficiency exhibited by BR compounds can be explained by two factors. On the one hand, it is important to recall that NR undergoes chain scission reactions during vulcanization (Figure 3), therefore competing cross-linking and scission reduce the vulcanization efficiency considerably. On the other hand, BR seems to favor the radical addition (polymerization) pathway as opposed to the termination (recombination) reaction. There are several factors that favor the addition of peroxides: peroxide concentration, vulcanization temperature and polymer backbone structure.[15,16] In this work, the two first two factors are invariant; therefore, the different behavior must again be ascribed exclusively to the chemical structure of polymer. There are three characteristics that support this supposition:

(i) The double bond/allylic hydrogen ratio. Polymeric radicals can react with neutral (nonradical) polymer chains via abstraction or via addition. The former is an inefficient reaction where the radical is transferred from one chain to the other without creation of a cross-link. The latter generates an effective junction by addition of the macro-radical to the double bond on another polymer chain, plus a new radical. In *cis*-BR the allylic/double-bond hydrogen ratio is 4/1 (this ratio is increased for higher proportions of more reactive vinyl segments), whereas NR has more allylic hydrogens (7/1) because of its methyl group, shifting the probability for an effective reaction toward BR without invoking any reaction between macro-radicals.

(ii) Steric effects. The methyl group in NR could exert some steric hindrance to the addition to the double bond as compared to *cis*-BR.

(iii) Hyperconjugation. This effect is favored in NR radicals, increasing the stability of allylic radicals and reducing their reactivity.

1.3. Cross-Link Distribution. Different reactions that take place during the vulcanization process not only lead to variations in the overall number of cross-links, but also in their spatial distribution. Figure 5 represents the ratio between the standard deviation and the average of the assumed

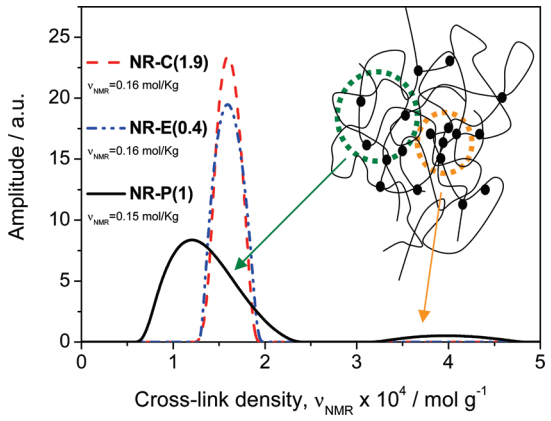

Figure 6. Effect of vulcanization systems on the distribution of cross-link density in NR samples. Note that samples have the same average cross-link density.

Gaussian spatial distribution of local cross-link density in the studied networks (i.e., the distribution width).

These results identify three factors that determine the cross-links distribution in rubber networks: the vulcanization system, the cross-link density (given by the concentration of curatives) and the polymer backbone structure. It is important to note that some other factors that we kept invariant, such as the vulcanization temperature, could also have an important influence on the cross-links distribution.[16]

For sulfur-based systems, it appears that most homogeneous rubbers are obtained for natural rubber, but note that we cannot fully exclude at this point that differences in the local spin dynamics among the individual protons in the different monomers, or microstructural variations (*trans*-1,4 or *vinyl* units) could also account for this small difference, as these factors also affect the shape of the analyzed NMR signal function.[59] A clear trend is the one related to the cross-link density, where a minimum (high homogeneity) is found at cross-link densities of around 2×10^{-4} mol/g. Here, competing effects such as the curative distribution after mixing, the time-scale of cross-linking vs (more and more hindered) diffusion of the active species during cross-linking, or a decreasing contribution of topological cross-links (entanglements) may be invoked for an explanation.

Most prominently, samples vulcanized with peroxides always show significantly broader distributions than the vulcanizates cured with sulfur, independently of the cross-link density or the type of polymer. This means that peroxide vulcanization, based on a radical pathway, generates more heterogeneous networks in comparison with the sulfur vulcanization. Using the numerical inversion procedures[57,58] discussed above and in the Appendix, it is possible to determine the actual spatial distribution function of cross-link density without any *a priori* assumption about its shape. Figure 6 shows the spatial cross-links distribution of three NR samples with similar (almost equal) average M_c but obtained using different vulcanization systems.

Whereas sulfur-based vulcanizates, e.g., NR-C and NR-E, do not show any difference and they are characterized by narrow Gaussian-like distributions of cross-links, i.e., they could be considered a random arrangement of cross-links forming very homogeneous networks, peroxide vulcanizates exhibit broader distributions, even with indications of bimodality.

During the peroxide vulcanization, the addition reaction of macro-radicals generates cross-links and new active peroxides that subsequently react with adjacent double bonds, similar to a polymerization reaction,[16,18] creating highly cross-linked areas (termed clusters[77]) embedded in a weakly cross-linked matrix. Figure 6 strongly supports the existence of this type of inhomogeneities in the networks vulcanized by peroxide, which are related with such "*polymerization*" reactions and the formation of highly cross-linked areas or clusters (represented by the fraction of rubber network defined by higher cross-link density). Although this mode of cross-linking does probably not dominate the overall vulcanization, the existence of such clusters could explain the drop in elastic properties found for peroxide vulcanizates in comparison with the more homogeneous sulfur networks.[16,78] Note that NR (from natural sources) and (synthetic) BR behave similarly in this context, stressing that the observed inhomogeneities of the rubber matrix are not specific to additional impurities in NR such as proteins and lipids. Of course, an influence of these components on the chain scission reactions discussed above cannot fully be excluded at this point.

We stress that these results are obtained *directly* by simultaneous molecular-scale observation of the behavior of all monomers in the rubber. The conclusions are thus essentially model free. However, these NMR results seems to be in contradiction to the speculative structures described by Ikeda et al. in a recent paper.[44] On the basis of strain-induced crystallization (SIC) studies, these authors found differences in the onset of SIC and the apparent lateral crystallite sizes upon stretching sulfur- and peroxide-vulcanized NR, and these differences were explained on the basis of assuming very homogeneous structures for peroxide-cured NR, yet even bimodal structures for sulfur-cured NR. Obviously, the experimental results are in some way related to the structure of the networks, but the observations bear no direct link to the real distribution of cross-links in the rubber matrix. Thus, the conjectures brought forth to rationalize the SIC behavior of these samples should be subject to revisions. In a more recent paper,[79] the same group used small-angle neutron scattering (SANS) on peroxide-cured natural rubber samples concludes that the structure of peroxide cross-linked NR is not homogeneous as it was previously described, and it is composed by several kinds of clusters with different sizes. In the same way, SIC behavior of NR vulcanizates with peroxide was then related to a progressive reduction of the overall size of inhomogeneities of these samples with the cross-link density. By using similar experimental procedures, they studied the effect of ZnO and other agents on the polyisoprene (IR) network structure vulcanized with sulfur.[43] They concluded that network structure of sulfur vulcanizates contains certain inhomogeneities, as it was also evidenced by other techniques such as transmission electron microscopy (TEM)[80] and magnetic resonance imaging (MRI).[81,82] One must of course keep in mind that we here address solely the cross-link density inhomogeneities of the actual rubber matrix, while scattering and direct imaging techniques as well as other indirect techniques also address inhomogeneities in the distribution of other minority components such as ZnO, residual sulfur, or proteins and lipids in the case of NR to different extents.

Considering the interesting SANS data,[43,79] which is based on changes observed upon swelling, we note that swelling is by itself a complex nonhomogeneous process, where excluded-volume effects, subaffine local deformations, and topological reorganization with a possible partial release of nontrapped entanglements ("desinterdispersion") all play a role and were of course considered by the authors. On the other hand, the NMR analysis of the samples from Figure 6 after swelling in toluene lead in all cases to very broad

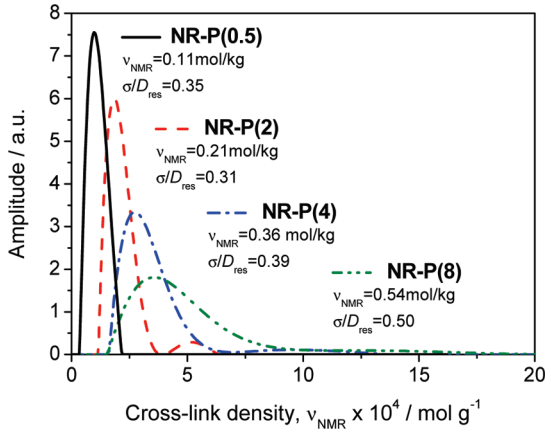

Figure 7. Effect of peroxide concentration on cross-links distribution in NR samples. Values of D_{res} and σ were obtained by assuming a Gaussian distribution and fitting experimental NMR data with eq 2.

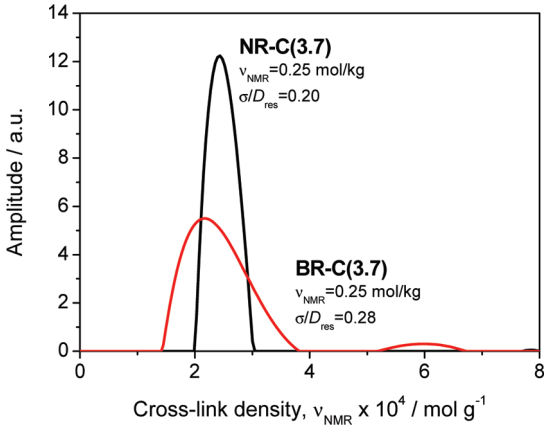

Figure 8. Difference between the cross-link distributions in NR and BR, both with similar average cross-link density and vulcanized with a conventional cure system. Values of ν_{NMR}, D_{res}, and σ used in the legend were obtained by fitting of the experimental NMR data with eq 2; hence, a Gaussian distribution was imposed.

distributions of dipolar couplings, completely covering up the significant differences between them, in agreement with our works on poly(dimethylsiloxane) networks.[83−85] This pinpoints that NMR analyses addressing matrix inhomogeneities should be performed on unswollen samples.

In order to address the differences between studies using SANS, TEM, and MRI and *apparent* contradictions with our NMR results, one needs to consider the length scales and the contrast mechanisms of the different techniques. First, the resolution in MRI[81,82] is very limited, obtaining information in the range of 10−100 μm at best. Contrast is often due to differences in T_2, which mainly reflects residual dipolar couplings, yet susceptibility contrast and effects from paramagnetic impurities may be relevant. SANS[43,79] was used to detect inhomogeneities in the range of 20−50 nm. In sulfur-cured polyisoprene rubber (IR) such inhomogeneities may partially be due to ZnO clusters, as found by TEM.[80] The present NMR study provides more local information, as spatial cross-linking inhomogeneities are detected on scales of several nanometers and above, where the lower limit is set by the length scale of dynamic averaging of monomers in different chains. In conclusion, based on the given literature one may conclude that NR (or IR) samples vulcanized with sulfur exhibit a rather homogeneous rubber matrix down to very local scales, with inhomogeneities at larger scales arising from the nonrubber components. In contrast, vulcanization with peroxides creates inhomogeneous network structures on all scales, because of specific radical reactions.

In order to more systematically address the significance of the "polymerization" pathway, Figure 7 shows cross-link density distributions for NR vulcanized with different amounts of peroxide. In this case, the addition reaction seems to be more favored at higher peroxide concentration.[15,16] At very low peroxide concentration (NR-P(0.5)), the sample shows a (relatively) broad distribution but no evidence of bimodality. A second component ("clusters") arises at higher content, and at some point (NR-P(8)), both components are broadened to such an extent that they merge into a single very broad distribution.

Finally, we shortly address the systematic differences between sulfur-cured BR and NR seen in Figure 5. Figure 8 indicates both a slightly broader major component and a weak bimodality for BR, and the bimodality was in fact found to increase at higher sulfur contents, in fact with both the conventional and the efficient system. As to the generally broader main peak, we again stress that this could be well due to slight differences in the NMR response of the different monomer units. The bimodality, however, is less easy to explain, in particular because of the lack of consensus concerning the nature of the reaction (ionic or free-radical) that governs the vulcanization. Nevertheless, just from the similarity with the peroxide behavior seen in Figure 6, the bimodality may be taken as an indication for radical reactions during sulfur-vulcanization of the more reactive BR.

Concluding this section, we point out that there are *a priori* reasons for the distribution of the NMR observable to be really broad to start with—in fact, simple arguments based on the Gaussian end-to-end distribution of the network chains suggest a broad γ distribution function of the residual coupling, and even more broadening should arise from the (most-probable) molecular weight distribution of the network chains, not even considering the (weak) variations along a network chain.[82] In contrast to all these predictions, all analyzed samples, even the most inhomogeneous ones, show narrower coupling distributions, and can in some cases even be well approximated by a single-valued distribution. An explanation of this very fundamental result, discussed in more detail in our recent papers,[54−85] comprises the cooperativity of the monomer fluctuations, the packing of different chains in the system and local force balances, which all reduce and homogenize the orientation fluctuations of monomers in connected network chains. This of course raises the question of the length scale, above which inhomogeneities can be observed as such. Detailed investigations are ongoing, and at the moment we can safely conclude that regions of sufficiently different average cross-link density must span a size scale of several network chain dimensions in order to exhibit a distinct behavior.

2. Rubber Segmental Dynamics. The structural differences analyzed in the previous sections may have consequences on the segmental dynamics. This is corroborated by the T_g data shown in Figure 9. T_g is always shifted to higher temperatures with increasing cross-link density, which is a well-known trend that is for instance explainable with additional stiffness arising from the cross-links. However, the dependence is different for the different vulcanization systems, and it is decisively nonlinear for the peroxide-based system. Note that dynamic-mechanical analysis of three samples vulcanized with different cure systems but similar cross-link density, the ones with ν_{NMR} around 4×10^{-4} mol/g, showed the same relative T_g variations within 0.1 K (data not shown).

Structural differences are certainly one possible explanation, but one has to keep in mind that some of the many

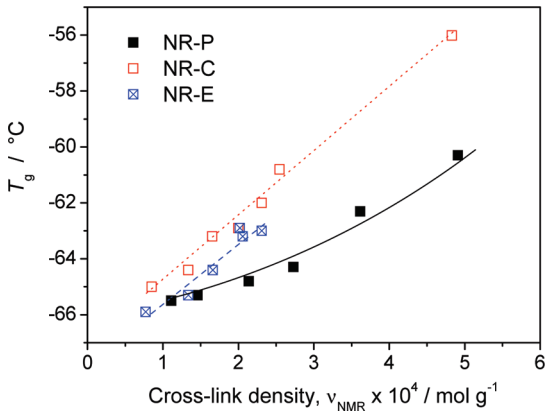

Figure 9. Relationship between the glass transition temperature (T_g) of NR samples vulcanized with different cure systems and the cross-link density.

components in the sulfur-based systems (stearic acid, accelerator) are small soluble organic molecules which can act as softening agents. This is, however, not a feasible explanation since the amount of curatives increases with the cross-link density. The small but relevant (1 K) shift between the efficient and the conventional system may arise from the different length of the (bulky) sulfur bridges that form the cross-links, and of course from the overall lower sulfur content in the latter.

It is even more difficult to explain the nonlinear variation of the peroxide-based system with curative content, as these systems have a comparably low content of a single curative, namely the peroxide, which is further expected to decompose upon vulcanization. The variations are therefore most probably due to the structural differences, and the substantial inhomogeneity evidenced by NMR may well be responsible. In particular, we believe that the large amount of potentially low-molecular weight defects (see Figure 3) plays a key role. Note that the shape (width) of the c_p step at T_g did not differ significantly among the samples, which means that the change in T_g occurs rather homogeneously throughout the samples.

For a closer analysis of the chain dynamics, we fitted the raw (non-normalized) DQ build-up and MQ decay data to eqs 4 and 5. As explained in this context, the correlation time τ_f represents a characteristic time scale of correlation loss due to localized chain modes. It is related to the fastest (Rouse) relaxation time of the system, and therefore it strongly depends on the segmental relaxation time and thus on T_g. We thus plot the results in Figure 10 vs the temperature difference to T_g, expecting comparable behavior.

The data in Figure 10 confirm that the dynamics speeds up upon heating, as of course expected. In the investigated range ($T - T_g \sim 70-75$ °C) and below, the $I_{\Sigma MQ}$ curves show the expected exponential relaxation behavior, yet at higher temperatures, more convex shapes are observed, and then, the data loses its sensitivity to the ever faster segmental fluctuations, and other factors dominate the decay.[49,56] We thus restrict the discussion to the lower temperature range.

A different behavior of the three vulcanization systems is again immediately indicated. Peroxide vulcanizates feature the apparently slowest overall dynamics at a given temperature (taking as reference the T_g of each sample), whereas NR-C have the fastest dynamics. NR-E samples seem to fall in-between these two systems, but without clear trend.

The apparent incongruence between the chain dynamics (τ_f) and the T_g in NR samples vulcanized with peroxide can be explained in two ways: a different fragility (i.e., the

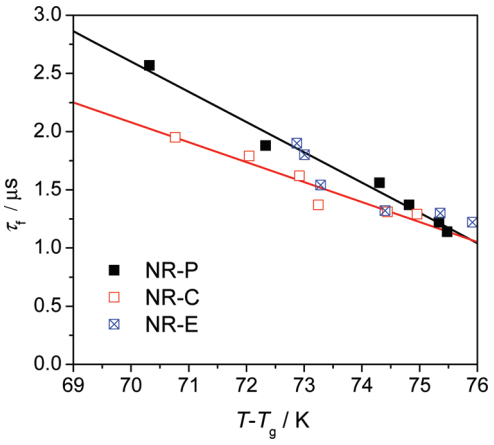

Figure 10. Variation of the apparent correlation time (τ_f) in NR samples cross-linked with different vulcanization systems as a function of temperature, scaled relative to the corresponding T_gs.

parameters in the WLF parameters), or by modified chain modes. Fragility could change for systems with different network structure and also with weak differences in composition. In addition, differences in the chain modes could be related again as a consequence of the substantial structural local inhomogeneities (involving highly cross-linked clusters) present in the peroxide-based systems. These aspects certainly deserve closer attention, such as detailed direct investigations of the temperature-dependence of the α process, and possibly normal-mode-related relaxations accessible by dielectric spectroscopy. We conclude that the effect of the decisive microstructural differences that we unveiled by NMR may significantly affect the dynamics and many other properties of the elastomers systems, and these correlations need to be uncovered before trying to use peroxide-cured rubbers as model systems for basic investigations in polymer physics.

Conclusions

MQ NMR spectroscopy performed on low-field spectrometers has been shown to be an inexpensive yet powerful tool to quantitatively investigate not only the structure, but also the chain dynamics of rubber networks. It was demonstrated that different vulcanization systems for dienic elastomers, here NR and BR, are characterized by different reaction pathways, leading to substantial variations in the fraction of elastically nonactive network defects, the vulcanization efficiency, the spatial distribution of cross-links, and the segmental dynamics. All these properties are ultimately relevant for an in-depth of the elastic properties of these compounds.

First, randomly cross-linked rubber networks contain some fraction of defects such as sol, dangling chains and loops. This fraction depends on temperature and the molecular weight between constraints, possibly due to slow arm retraction processes of chain ends, which explains that the defect content decreases rapidly with cross-link density for sulfur-based systems. However, we have found that peroxide-cured NR with reasonable cross-link density contains unexpectedly high amounts, on the order of 20 wt %, of such defects. This was explained by side reactions of the cross-linking process.

Focusing on the actual network component, the spatial distribution of cross-links also varies substantially between sulfur-based cure systems and peroxide vulcanization. While sulfur vulcanization of both NR and *cis*-BR generates rather homogeneous cross-link distributions in the rubber matrix on all scales down to a local level of a few nm, peroxide-cured systems exhibit a heterogeneous and even bimodal structure. These results can

again be explained via the radical mechanism that dominates peroxide vulcanization process, as it partially leads to polymerization-type cross-linking involving addition to the double bonds, leading to highly cross-linked clusters which we could observe directly.

A balance between radical cross-linking through recombination of macro-radicals and the mentioned addition/polymerization, and of course potential chain scission, determines the final structure of the network, which appears to depend strongly on the polymer backbone structure, as was demonstrated by comparing *cis*-BR and NR samples. The methyl group on the NR monomer and the associated tertiary carbon are probably responsible for much enhanced chain scission reaction and the largely increased defect content in comparison with BR. In addition, the methyl group stabilizes the macro-radical by hyperconjugation phenomena and may further exert some steric hindrance on the addition of macro-radicals to the double bond, which explains the much higher efficiency of peroxide linking in BR. However, the role of NR-specific impurities such as proteins and lipids that may interact with radicals remains to be clarified, best in terms of a comparison of NR and IR samples, which we leave for future work.

BR samples were in fact always found to be more inhomogeneous than NR samples, indicating that the tendency for the formation of macro-cross-links (clusters) via a chain reaction ("polymerization") may not only be relevant for peroxide-based cross-linking, but also to a limited degree in sulfur vulcanization.

The different network structures and defect contents obtained for the different vulcanization systems further leads to significant changes in the value and the cross-link density dependence of T_g. Networks obtained by peroxide vulcanization have the lowest T_g values, yet exhibit apparently slower chain modes in comparison with conventional vulcanizates. These results could be again explained by the much increased defect content, and by the inhomogeneous structures of these networks, respectively. To conclude, clear relationships between different vulcanization reactions, the network structure, and the properties of dienic elastomers emerge from their study by low-field MQ NMR spectroscopy, and more in-depth investigations of the properties of peroxide vulcanizates in relation to their substantial inhomogeneity is mandatory before continuing their use in basic investigations of rubber elastic phenomena.

Acknowledgment. J.L.V. wants to thank the Alexander von Humboldt Foundation for his fellowship as well as CSIC for his current JAE-Doc contract. Financial support from CICYT (MAT 2008-1073) is also gratefully acknowledged. We thank Dr. E. Hempel and PD Dr. M. Beiner (Martin-Luther Universität Halle-Wittenberg) for the DSC and dynamic-mechanical analyses, and for fruitful discussions.

Appendix: Improved Regularization Procedure

In the original version of the modified regularization program FTIKREG for the estimation of coupling distributions, originally published by Weese,[57,58] an inverted-Gaussian single-D_{res} build-up function (eq 2 with $\sigma = 0$),

$$I_{nDQ}(D_{res}) = \frac{1}{2}\left(1 - \exp\left[-\frac{2}{5}(D_{res})^2 {\tau_{DQ}}^2\right]\right) \qquad (6)$$

was used as a kernel function. The selection of eq 6 as kernel function, in combination with the restrictuion to fit only the initial build-up (see below) created a problem in the final normalized DQ intensity. It must always reach 0.5 since it contains half of the excited quantum orders in the long-time limit. For this reason, on needed to add long-time data points with $I_{nDQ} = 0.5$ to externally enforce the best-fit I_{nDQ} to reach the expected plateau. Since FTIKREG was initially conceived for inverse Laplace transformations (i.e., using a falling exponential as kernel function), it has a built-in option to enforce $I = 0$ in the long-time limit. In order to use this option and obviate the use of an arbitrary number of additional points, the program now internally fits *decay* data of the form $0.5 - I_{nDQ}$ to a falling Gaussian, $0.5 \times e^{-2/5(D_{res})2}{\tau_{DQ}}^2$.

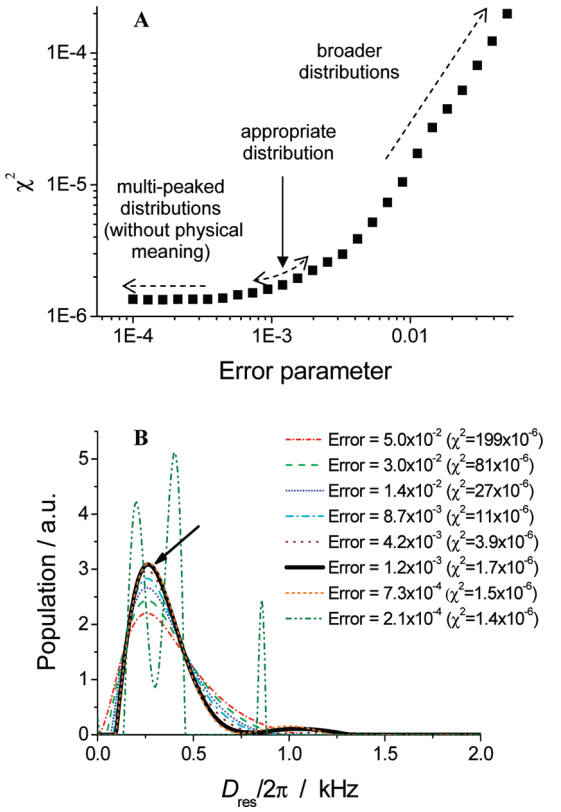

Figure 11. (A) χ^2 as a function of input error in FTIKREG program. (B) Distributions of D_{res} as a function of input error (and χ^2) for NR sample vulcanized with dicumyl peroxide (3 parts per hundred of rubber). The resulting distributions become broader with increasing input error, and become multiply peaked at too low values. The solid arrow in A indicates the most realistic error parameter to give the bold distribution curve in B, which does not change significantly over the range pointed out in A.

Further, in very homogeneous samples, one observes a slight maximum in the I_{nDQ} build-up curve (see Figure 1D). It cannot be represented by the inverted-Gaussian function, eq 6, therefore the latter is only an approximation of true data. This is in fact why experimental data was only fitted up to $I_{nDQ} < 0.45$ (equating this value with eq 6 yields a definition of the fitting limit $\tau_{DQ}^{max} = 2.4/D_{res}$), which is the region of good agreement. To reflect the observed full shape of a build-up curve and thus obtain more reliable results for wider or multimodal distributions, a new empirical kernel function derived from experiments on different, very homogeneous elastomer samples has been implemented (details will be reported in an upcoming publication):

$$I_{nDQ} = 0.5 \times (1 - \exp(-(0.378 \times D_{res})^{1.5} {\tau_{DQ}}^{1.5}) \cos(0.583 \times D_{res}\tau_{DQ})) \qquad (7)$$

Another central improvement implemented in the modified regularization procedure concerns the error parameter that is required by FTIKREG. This parameter should reflect the constant, absolute-scale statistical error associated with the data

points, and is needed for a proper initialization of the regularization parameter. The error parameter thus affects the smoothing of the data and the number of distribution modes extracted from the data, therefore a proper selection of the error parameter is necessary to obtain a meaningful representation of the dipolar coupling distribution. Too low values commonly lead to an "overinterpretation" in terms of too many modes. The actual problem is that the error associated with the data is not constant. At longer times the experimental intensities (DQ and reference, I_{DQ} and I_{ref}, respectively) are close to be completely relaxed, which is why the point-by-point normalized data arising from the quotient exhibits an increasing uncertainty.

In order to select an error parameter that leads to a physically realistic distribution, the program now automatically varies the error parameter over a given range, and outputs the distributions for each value, along with the corresponding χ^2 value (mean squared deviation between data and fit). See Figure 11, parts A and B, for the variation of χ^2 with the given error parameter for a typical natural rubber (NR) network, and the resulting distributions. We take the most realistic distribution (shown as thick solid line in Figure 11) as the one with the lowest error parameter below which χ^2 saturates at a nearly constant value. In most cases, lower error parameter values lead to multiply peaked distributions, which however do not lead to better overall fits (thus not lowering χ^2 significantly), and are consequently not physically meaningful.

References and Notes

(1) Alliger, G.; Sjothun, I. J. *Vulcanization of Elastomers*; Reinhold Publishing Corp.: New York, 1964.
(2) Hofmann, W. *Vulcanization and vulcanizing Agents*; MacLaren: London, UK. 1967.
(3) Chapman, A.V.; Porter, M. *Natural Rubber Science and Technology*; Oxford Science Publications: New York, 1988.
(4) Coran, A. Y. *Rubber Chem. Technol.* **1995**, *68*, 351–375.
(5) Aprem, A. S.; Joseph, K.; Thomas, S. *Rubber Chem. Technol.* **2005**, *78*, 458–488.
(6) Coleman, M. M.; Shelton, J. R.; Koenig, J. L. *Ind. Eng. Chem. Product Res. Dev.* **1974**, *13*, 154–165.
(7) Krejsa, M. R.; Koenig, J. L. *Rubber Chem. Technol.* **1993**, *66*, 376–410.
(8) Akiba, M.; Hashim, A. S. *Prog. Polym. Sci.* **1997**, *22*, 475–521.
(9) Heideman, G.; Datta, R. N.; Noordermeer, J. W. M. *Rubber Chem. Technol.* **2004**, *77*, 512–541.
(10) Ghosh, P.; Katare, S.; Patkar, P.; Caruthers, J. M.; Venkatasubramanian, V. *Rubber Chem. Technol.* **2003**, *76*, 592–693.
(11) Manik, S. P.; Banerjee, S. *Rubber Chem. Technol.* **1970**, *43*, 1311–1326.
(12) Brydson, J. A. *Rubber Chemistry*; Applied Science Publishers, Ltd.: London, England. 1978.
(13) Gonzalez, L.; Rodriguez, A.; del Campo, A.; Marcos-Fernandez, A. *Rubber Chem. Technol.* **2000**, *73*, 89–100.
(14) Posadas, P.; Fernandez, A.; Brasero, J.; Valentin, J. L.; Marcos, A.; Rodriguez, A.; Gonzalez, L. *J. Appl. Polym. Sci.* **2007**, *106*, 3481–3487.
(15) Dluzneski, P. R. *Rubber Chem. Technol.* **2001**, *74*, 451–492.
(16) Valentin, J. L.; Fernandez-Torres, A.; Posadas, P.; Marcos-Fernandez, A.; Rodriguez, A.; Gonzalez, L. *J. Polym. Sci., Part B: Polym. Phys.* **2007**, *45*, 544–556.
(17) Hernandez, L. G.; Diaz, A. R.; Fernandez, A. M.; Anton, C. C. *Kautsch. Gummi Kunstst.* **1994**, *47* (10), 715–721.
(18) Gonzalez, L.; Rodriguez, A.; Marcos, A.; Chamorro, C. *Rubber Chem. Technol.* **1996**, *69*, 203–214.
(19) Treloar, L. R. G. *The Physics of Rubber Elasticity*, 3rd ed.; Clarendon Press: Oxford, U.K., 1975.
(20) Mark, J. E.; Erman, B.; Eirich, F. R. *Science and Technology of Rubber*, 2nd ed.; Academic Press: San Diego, CA, 1994.
(21) Rubinstein, M.; Colby, R. H. *Polymer Physics*; Oxford University Press: New York. 2003.
(22) Kuhn, W.; Grün, F. *Kolloid Z. Z. Polym.* **1943**, *101*, 248–262.
(23) James, H. M.; Guth, E. *J. Chem. Phys.* **1943**, *11*, 455–481.
(24) James, H. M.; Guth, E. *J. Chem. Phys.* **1947**, *15*, 669–683.
(25) Flory, P. J.; Gordon, M.; McCrum, N. G. *Proc. R. Soc. London A* **1976**, *351*, 351–380.
(26) Flory, P. J.; Erman, B. *Macromolecules* **1982**, *15*, 800–806.
(27) Erman, B.; Flory, P. J. *Macromolecules* **1982**, *15*, 806–811.
(28) Edwards, S. F. *Proc. Phys. Soc.* **1967**, *92*, 9–16.
(29) Rubinstein, M.; Panyukov, S. *Macromolecules* **1997**, *30*, 8036–8044.
(30) Ball, R. C.; Doi, M.; Edwards, S. F.; Warner, M. *Polymer*. **1981**, *22*, 1010–1018.
(31) Edwards, S. F.; Vilgis, T. A. *Rep. Prog. Phys.* **1988**, *51*, 243–297.
(32) Rubinstein, M.; Panyukov, S. *Macromolecules* **2002**, *35*, 6670–6686.
(33) Vilgis, T. A. *Macromolecules* **1992**, *25*, 399–403.
(34) Vilgis, T. A.; Heinrich, G. *Macromol. Theory Simul.* **1994**, *3*, 271 – 293.
(35) Tan, Z.; Jaeger, R.; Vancso, G. J. *Polymer* **1994**, *35*, 3230–3236.
(36) Arndt, K. F.; Schreck, J. *Acta Polym.* **1985**, *36*, 56–57.
(37) Gillmor, J. R.; Colby, R. H.; Patel, S. K.; Malone, S.; Cohen, C. *Macromolecules* **1992**, *25*, 5241–5251.
(38) Valentin, J. L.; Carretero-Gonzalez, J.; Mora-Barrantes, I.; Chasse, W.; Saalwächter, K. *Macromolecules* **2008**, *41*, 4717–4729.
(39) Pyckout-Hintzen, W.; Springer, T.; Forster, F.; Gronski, W. *Macromolecules* **1991**, *24*, 1269–1274.
(40) Zaper, A. M.; Koenig, J. L. *Rubber Chem. Technol.* **1987**, *60*, 252–277.
(41) Orza, R. A.; Magusin, P. C. M. M.; Litvinov, V. M.; van Duin, M.; Michels, M. A. J. *Macromolecules* **2009**, *42*, 8914–8924.
(42) Imanishi, Y.; Adachi, K.; Kotaka, T. *J. Chem. Phys.* **1988**, *89*, 7585–7592.
(43) Ikeda, Y.; Higashitani, N.; Hijikata, K.; Kokubo, Y.; Morita, Y.; Shibayama, M.; Osaka, N.; Suzuki, T.; Endo, H.; Kohjiya, S. *Macromolecules* **2009**, *42*, 2741–2748.
(44) Ikeda, Y.; Yasuda, Y.; Hijikata, K.; Tosaka, M.; Kohjiya, S. *Macromolecules* **2008**, *41*, 5876–5884.
(45) Litvinov, V. M.; De, P. P. *Spectroscopy of Rubbers and Rubbery Materials*; Rapra Technology Ltd.: Shawbury, U.K., 2002.
(46) Cohen-Addad, J. P.; Vogin, R. *Phys. Rev. Lett.* **1974**, *33*, 940–943.
(47) Brereton, M. G. *Macromolecules* **1990**, *23*, 1119–1131.
(48) Graf, R.; Heuer, A.; Spiess, H. W. *Phys. Rev. Lett.* **1998**, *80*, 5738–5741.
(49) Saalwächter, K. *Prog. Nucl. Magn. Reson. Spectrosc.* **2007**, *51*, 1–35.
(50) Litvinov, V. M. *Macromolecules* **2006**, *39*, 8727–8741.
(51) Callaghan, P. T.; Samulski, E. T. *Macromolecules* **1997**, *30*, 113–122.
(52) Demco, D. E.; Hafner, S.; Fülber, C.; Graf, R.; Spiess, H. W. *J. Chem. Phys.* **1996**, *105*, 11285–11296.
(53) Saalwächter, K. *Macromolecules* **2005**, *38*, 1508–1512.
(54) Saalwächter, K.; Sommer, J.-U. *Macromol. Rapid Commun.* **2007**, *28*, 1455–1465.
(55) Saalwächter, K.; Ziegler, P.; Spyckerelle, O.; Haidar, B.; Vidal, A.; Sommer, J.-U. *J. Chem. Phys.* **2003**, *119*, 3468–3482.
(56) Saalwächter, K.; Heuer, A. *Macromolecules* **2006**, *39*, 3291–3303.
(57) Weese, J. *Comput. Phys. Commun.* **1992**, *69*, 99–111.
(58) Weese, J. *Comput. Phys. Commun.* **1993**, *77*, 429–440.
(59) Saalwächter, K.; Herrero, B.; López-Manchado, M. A. *Macromolecules* **2005**, *38*, 9650–9660.
(60) Curro, J. G.; Pincus, P. *Macromolecules* **1983**, *16*, 559–562.
(61) Heinrich, G.; Vilgis, T. A. *Macromolecules* **1992**, *25*, 404–407.
(62) Roth, L. E.; Vega, D. A.; Valles, E. M.; Villar, M. A. *Polymer*. **2004**, *45*, 5923–5931.
(63) Batra, A.; Cohen, C.; Archer, L. *Macromolecules* **2005**, *38*, 7174–7180.
(64) Doi, M.; Edwards, S. F. *The Theory of Polymer Dynamics*; Clarendon Press: Oxford, U.K., 1986.
(65) Pearson, D. S.; Helfand, E. *Macromolecules* **1984**, *17*, 888–895.
(66) Plazek, D. J. *J. Polym. Sci. Polym. Phys.* **1966**, *4*, 745–763.
(67) Dickie, R. A.; Ferry, J. D. *J. Phys. Chem.* **1966**, *70*, 2594–2600.
(68) Acosta, R. H.; Vega, D. A.; Villar, M. A.; Monti, G. A.; Valles, E. M. *Macromolecules* **2006**, *39*, 4788–4792.
(69) Acosta, R. H.; Monti, G. A.; Villar, M. A.; Valles, E. M.; Vega, D. A. *Macromolecules* **2009**, *42*, 4674–4680.
(70) Moore, C. G.; Scanlan, J. *J. Polym. Sci.* **1960**, *43*, 23–33.
(71) Heinen, W.; Rosenmöller, C. H.; Wenzel, C. B.; de Groot, H. J. M.; Lugtenburg, J.; van Duin, M. *Macromolecules* **1996**, *29*, 1151–1157.
(72) Coiai, S.; Passaglia, E.; Aglietto, M.; Ciardelli, F. *Macromolecules* **2004**, *37*, 8414–8423.
(73) Graessley, W. W. *Adv. Polym. Sci.* **1974**, *16*, 1–177.
(74) Abdel-Goad, M.; Pyckhout-Hintzen, W.; Kahle, S.; Allgaier, J.; Richter, D.; Fetters, L. J. *Macromolecules* **2004**, *37*, 8135–8144.

(75) Mark, J. E. *Polymer Data Handbook*; Oxford University Press, Inc.: New York, 1999.
(76) Skinner, T. D. *Rubber Chem. Technol.* **1972**, *45*, 182–192.
(77) Mark, H. F. *Rubber Chem. Technol.* **1988**, *61*, G73.
(78) Gonzalez, L.; Valentin, J. L.; Fernandez-Torres, A.; Rodriguez, A.; Marcos-Fernandez, A. *J. Appl. Polym. Sci.* **2005**, *98*, 1219–1223.
(79) Suzuki, T.; Osaka, N.; Endo, H.; Shibayama, M.; Ikeda, Y.; Asai, H.; Higashitani, N.; Kokubo, Y.; Kohjiya, S. *Macromolecules* **2010**, *43*, 1556–1563.
(80) Dohi, H.; Horiuchi, S. *Polymer* **2007**, *48*, 2526–2530.
(81) Rana, M. A.; Koenig, J. L. *Macromolecules* **1994**, *27*, 3727–3734.
(82) Oh, S. J.; Koenig, J. L. *Polymer*. **1999**, 4703–4708.
(83) Sommer, J.-U.; Saalwächter, K. *Eur. Phys. J. E.* **2005**, *18*, 167–182.
(84) Saalwächter, K.; Kleinschmidt, F.; Sommer, J.-U. *Macromolecules* **2004**, *37*, 8556–8568.
(85) Sommer, J.-U.; Chassé, W.; Valentin, J. L.; Saalwächter, K. *Phys. Rev. E.* **2008**, *78*, 051803.